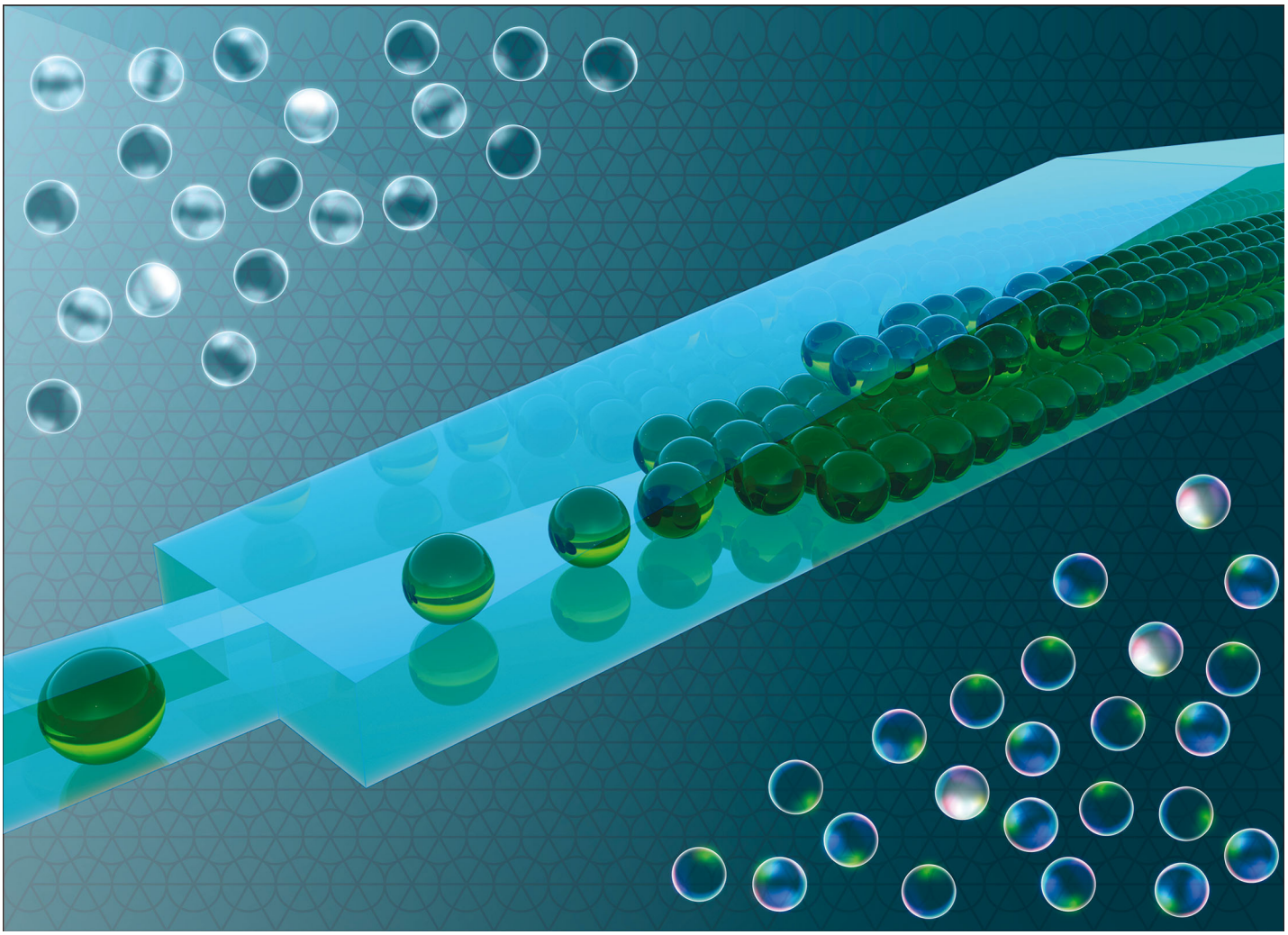

Showcasing research from Professor Michinao Hashimoto's laboratory, Pillar of Engineering and Product Development, Singapore University of Technology and Design, Singapore; in collaboration with Professor Patrick S. Doyle's laboratory, Department of Chemical Engineering, Massachusetts Institute of Technology, Massachusetts, USA.

Self-assembly of droplets in three-dimensional microchannels

Three dimensional microchannels were used to self-assemble droplets into ordered two- and three-dimensional arrays. The use of microchannels with axial gradients in height enabled self-assembly of emulsions at low volume fractions. Self-assembly of ordered emulsions was highly path dependent – it was governed by transitions in the cross-sectional shapes of the microchannel and not the final geometry of the microchannel. The self-assembled droplets were subsequently used as templates in the fabrication of porous hydrogel fibres with anisotropic internal structure.

As featured in:

See Michinao Hashimoto *et al.*, *Soft Matter*, 2019, **15**, 4244.

ROYAL SOCIETY OF CHEMISTRY | Celebrating IYPT 2019

rsc.li/soft-matter-journal

Registered charity number: 207890

Soft Matter

COMMUNICATION

Self-assembly of droplets in three-dimensional microchannels

Pravien Parthiban,[ab] Patrick S. Doyle [b] and Michinao Hashimoto *[a]

Cite this: *Soft Matter*, 2019, 15, 4244

Received 12th November 2018, Accepted 11th April 2019

DOI: 10.1039/c8sm02305k

rsc.li/soft-matter-journal

Self-assembly of droplets guided by microfluidic channels have potential applications ranging from high throughput assays to materials synthesis, but such demonstrations have been limited primarily to two-dimensional (2D) assembly of droplets in planar microfluidic devices. We demonstrated the use of three-dimensional (3D) microchannels to self-assemble droplets into ordered 2D and 3D arrays by designing microchannels with axial gradients in height and controlling the volume fraction of the droplets in the channel. In contrast to previous demonstrations, ordered 2D arrays of droplets were assembled at low volume fractions of the dispersed phase. Interestingly, we found that the self-assembly of droplets in microchannels was highly path dependent. The assembly of droplets was governed by transitions in the cross-sectional shapes of the microchannel, not the final geometry of the chamber for the assembly of droplet, which is a hitherto rarely explored phenomenon. The assembled droplets were used as templates for the fabrication of millimeter scale, anisotropic hydrogel fibers with ordered pore sizes (~250 μm). These demonstrations suggested that 3D microchannels would be a viable platform for the manipulation of droplets, and applicable for the continuous synthesis of complex materials with 3D morphologies.

Introduction

This paper describes the tunable self-assembly of microfluidic droplets into three-dimensional (3D) ordered arrays guided by microchannels with axial gradients in height. Microfluidics allows facile, tunable generation of highly monodisperse bubbles and droplets, and dynamic assembly of these bubbles and droplets into ordered foams and emulsions.[1–12] The self-assembled flowing lattices of droplets and bubbles can be readily reorganized and manipulated in microchannels.[13,14] Self-assembly of droplets and bubbles in microchannels has elicited much interest as it is a simple platform to study non-equilibrium self-assembly[15] and many-body systems.[16] Microfluidic assembly of droplets and bubbles are used in a wide range of applications including high throughput analysis,[17–19] synthesis of nanoparticles,[20] fabrication of reconfigurable optical materials,[8,21] fabrication of networks of droplet interface bilayers,[22,23] and investigation of the transport of multiphase flows in porous media.[24–27] Crucially, the microfluidic self-assembly of flowing lattices of bubbles and droplets is widely viewed as a viable platform for the design and engineering of complex, multiphase, multicomponent, hierarchical materials.[2,6,7,10–12,28,29] As such, the predictable and tunable self-assembly of bubbles and droplets in microchannels has attracted significant attention over the past decade.

To date, most studies on the microfluidic self-assembly of bubbles and droplets have used two dimensional (2D) microchannels. Here, we define 2D or planar microchannels as those with uniform height, and conversely, we define 3D microchannels as those that have varying heights. Microchannels used in past studies on the self-assembly of bubbles and droplets were engineered primarily out of poly(dimethylsiloxane) (PDMS) using molds patterned with photolithography (called masters or templates). Fabrication of molds with various or gradually changing heights would require a multi-step and/or gray scale photolithography that is laborious. Thus, barring a few exceptions,[3,6,9,30] all microchannels used in past studies of microfluidic self-assembly of droplets and bubbles have been 2D in nature.[1,2,4,5,7,8,10–12,15,16]

In this paper, enabled by 3D printing of soft lithography molds, we demonstrated the controlled self-assembly of droplets in 3D microchannels. Past studies have shown that droplets or bubbles generated in microchannels self-assemble into 2D lattices only at high volume fractions of the dispersed phase (ϕ_D).[1–12] In this work, we demonstrated that in microchannels with axial gradients in height, 2D lattices of droplets can be self-assembled even at low ϕ_D. To the best of our knowledge this is the first demonstration of in-channel self-assembly of droplets at low ϕ_D. Furthermore, 3D lattices of droplets were readily

[a] *Pillar of Engineering Product Development, Singapore University of Technology and Design, 8 Somapah Road, 487372, Singapore. E-mail: hashimoto@sutd.edu.sg*

[b] *Department of Chemical Engineering, Massachusetts Institute of Technology, 77 Massachusetts Ave, Cambridge, MA 02139, USA*

self-assembled by systematically increasing ϕ_D. Previous investigations have shown that the structure of the self-assembled lattices of droplets or bubbles depends on the size of the microchannel, the size of the droplet or bubble, and the volume fraction of the dispersed phase.[2–4,6–9,17,31] Interestingly, in our experiments droplet self-assembly in 3D microchannels was also dependent on how they were assembled (*i.e.* path dependence); the self-assembly of droplets was governed by the transitions in the geometry of microchannels, and not the final geometry of the microfluidic chamber. Specifically, droplets self-assembled into ordered arrays in microchannels with a linear gradual increase in height. In contrast, at identical operating conditions, self-assembly into ordered arrays did not occur in microchannels when the increase in height occurred in a single step change.

As a potential application, self-assembled 2D lattices of droplets in 3D microchannels were used as a template to continuously synthesize macroporous hydrogel fibers. The use of 3D microchannels enabled the self-assembly of 2D lattices of droplets at low volume fractions of the droplets, which allowed the extruded microfibers to have structural anisotropy. The ordered macropores were confined to a single surface within the fiber. Our demonstrations suggested that 3D microchannels with appropriate designs would enable to manipulate assembly of droplets in 2D and 3D, and such control over the self-assembly should be useful for synthesis of complex materials with 3D internal morphologies.

Results and discussions

Self-assembly of 2D lattices of droplets – 2D *vs.* 3D microchannels

In microfluidic self-assembly of bubbles and droplets into ordered arrays, the droplets and bubbles are typically generated at a flow-focusing or T-junction geometry. The generated droplets and bubbles subsequently flow into a wider microchannel. At high volume fractions of the dispersed phase, the droplets and bubbles jam and self-assemble into 2D lattices in the horizontal plane.[1–12]

Different topologies of ordered emulsions and foams have been obtained by varying the size and volume fraction of the dispersed phase in 2D microchannels.[2–4,6–9,17,31] In 2D microchannels, there is a change in width and no change in height. In such microchannels, 2D lattices of droplets form only at high volume fractions of the dispersed phase.[1,2,4,5,7,8,10–12,15,16] The utility of 2D microchannels in the self-assembly of ordered emulsions is therefore limited by a narrow range of experimental parameters (*i.e.* rates of flows of continuous and dispersed phases). High volume fractions of the dispersed phase (ϕ_D) is achieved by injecting a high fraction of the dispersed phase into the channel. The volume fraction of the dispersed phase (ϕ_D), is typically calculated as $\phi_D = V_{D,total}/V_{CH}$, where $V_{D,total}$ is the total volume of the droplets in the microchannel, and V_{CH} is the volume of the microchannel. In the flow of foams or emulsions, ϕ_D is not identical to the fraction of the injected dispersed phase (α_D), calculated as $\alpha_D = Q_D/(Q_D + Q_C)$, where Q_D is the total flow rate of the injected dispersed phase and Q_C is the total flow rate of the injected continuous phase. The values of ϕ_D and α_D differ because the continuous phase can flow at higher velocity than the droplets or bubbles in the flow of emulsions or foams.[2,28] Typically ϕ_D is greater than α_D.

We hypothesized that self-assembly of droplets would be facilitated by appropriate design of the geometry of the microchannel and can be achieved at low α_D. In this section, we tested the self-assembly of droplets in 2D and 3D microchannels. In the 2D microchannel, there is only a lateral change in dimension at the region of expansion, while in the 3D microchannel the dimensions change in both the lateral and vertical directions at the region of expansion.

We compared the ability of 2D and 3D microchannels to facilitate the self-assembly of droplets into 2D lattices for varying α_D. The schematic of the experimental set up is shown (Fig. 1a and b), and details of the experiment are provided in Materials and methods. Water droplets in hexadecane were generated at a T-junction. Hexadecane containing a dissolved surfactant was used as the continuous phase to prevent the coalescence of the water droplets. The droplets flowed into the section where the width of the microchannel was increased to 2 mm. Self-assembly of droplets was designed to take place in this section. We compared two types of microfluidic devices, namely the 2D and 3D devices. In the 2D device, the entire microfluidic device had a constant height of 0.5 mm (Fig. 1a). In the 3D device, the width was increased to 2 mm in a single step, and the height was linearly increased from 0.5 mm to 2 mm over a length of 10 mm (Fig. 1b). Droplets of water in hexadecane were generated at Q_{O1} = 25 μL min^{-1} and Q_W = 5 μL min^{-1}, and α_D was decreased by increasing Q_{O2} from 0 to 75 μL min^{-1}. α_D, the fraction of the injected dispersed phase was calculated as $\alpha_D = Q_W/(Q_W + Q_{O1} + Q_{O2})$. We studied the self-assembly of droplets at α_D = 0.167, 0.091, 0.063, 0.048. We found that, at all experimental conditions, the 2D device did not promote the self-assembly of droplets into ordered lattices. In contrast, at the same flow rates of water and hexadecane, *i.e.* at same α_D, the 3D device promoted the self-assembly of droplets into ordered 2D hexagonal lattices (Fig. 1c–f). In the 3D device, the droplets were unconfined; the diameter of droplets was less than the height of the microchannel. The aqueous droplets settled down to the bottom of the microchannel as their density was higher than that of hexadecane (0.77 g cm^{-3}). Thus, the droplets accumulated at the bottom of the channel where they jammed and assembled into ordered structures. We estimated ϕ_D from the microscopic images of the droplet flow in 2D and 3D microchannels (Fig. 1c–f). ϕ_D, the volume fraction of the dispersed phase was calculated as $\phi_D = nV_D/Lwh$, where n is the number of droplets in length L of the microchannel, V_D is the volume of a single droplet, and w, h, are the widths and heights of the microchannel. In 2D microchannels, the droplets were confined by the top and bottom walls of the microchannel and took on a pancake like shape; in the 3D microchannel, the droplets were unconfined and were spherical in shape. V_D in the 2D microchannels was

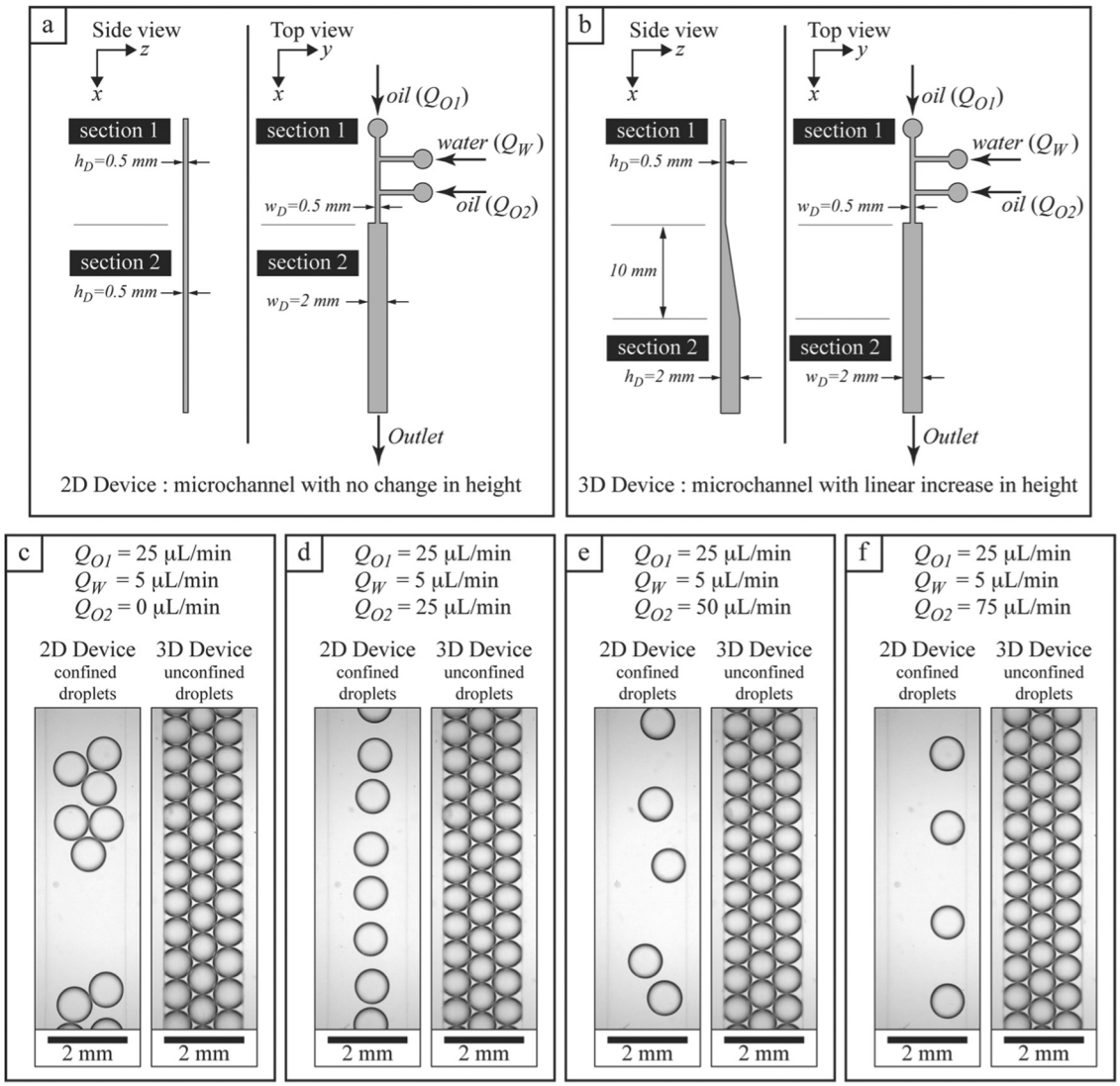

Fig. 1 (a and b) Schematic illustrations of 2D and 3D microfluidic devices used to study the self-assembly of microfluidic droplets into 2D arrays. (c–f) Microscopic images of self-assembled droplets in section 2 of the 2D and 3D microfluidic device at α_D = 0.167, 0.091, 0.063, 0.048. In the 2D microchannels, $\phi_D \sim$ 0.29, 0.22, 0.18, 0.14. In the 3D microchannels, $\phi_D \sim$ 0.18 for all α_D. Droplets were generated at the same flow rates of oil and water. Additional oil was introduced from the second oil inlet to decrease α_D. The photomicrographs suggested that the 3D microfluidic device promoted the self-assembly of 2D droplet arrays over a wide range of α_D. In contrast, with the 2D microfluidic device, at the same α_D, self-assembly of droplets into 2D arrays was not observed.

estimated as a volume of cylinder with diameter d, and height h. V_D in the 3D microchannels was calculated as the volume of a sphere of diameter d. d was measured directly from the microscopic images of the droplets. In the 2D microchannels for α_D = 0.167, 0.091, 0.063, 0.048, the measured ϕ_D were 0.29, 0.22, 0.18, and 0.14. Herein, ϕ_D was linearly dependent on α_D. In contrast, with the 3D microchannel at all values of α_D, the measured ϕ_D was 0.18. These observations implied that in 3D microchannels the difference in average velocity between the continuous phase and the droplets increased as α_D was decreased, favoring the self-assembly of ordered lattices. To the best of our knowledge, this is the first demonstration of self-assembly of droplets at low ϕ_D. We note that this self-assembly at low ϕ_D is not predicted by past theoretical studies.[4,17,31]

Critical α_D required for self-assembly

In the previous section, we demonstrated that 3D microchannels can facilitate the self-assembly of droplets at low fractions of the injected dispersed phase α_D. In this section we determined the critical α_D required for self-assembly of water droplets in 3D microchannels. Water droplets in hexadecane were generated at a T-junction by pumping in water at a flow rate of Q_W and hexadecane at a flow rate of Q_{O1}. Hexadecane containing a dissolved surfactant was used as the continuous phase to prevent the coalescence of the water droplets. Additional hexadecane was injected at a flowrate Q_{O2} to further reduce α_D, where $\alpha_D = Q_W/(Q_W + Q_{O1} + Q_{O2})$. The generated droplets flowed into a section where the width was increased from 0.5 mm to 2 mm in a single step and the height was linearly increased from 0.5 mm

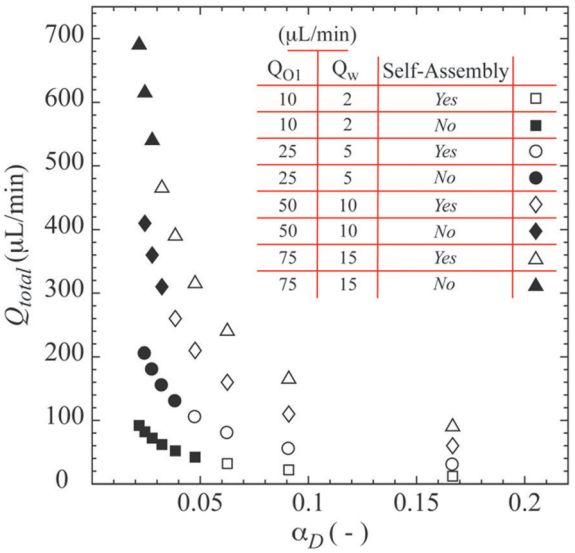

Fig. 2 The total flow rate $Q_{total} = Q_W + Q_{O1} + Q_{O2}$ is plotted against the injected fraction of the dispersed phase $\alpha_D = Q_W/Q_{total}$ for the self-assembly of droplets in 3D microchannels. Droplets were generated at Q_W = 2 μL min^{-1} and Q_{O1} = 10 μL min^{-1} (square symbols), Q_W = 5 μL min^{-1} and Q_{O1} = 25 μL min^{-1} (circle symbols), Q_W = 10 μL min^{-1} and Q_{O1} = 50 μL min^{-1} (diamond symbols), Q_W = 15 μL min^{-1} and Q_{O1} = 75 μL min^{-1} (triangle symbols). In each case α_D was decreased by increasing Q_{O2} resulting in an increase in Q_{total}. The unfilled symbols represent conditions were self-assembly occurred, and the black filled symbols represent conditions were self-assembly did not occur. The self-assembly occurred at lower α_D when droplets were generated at higher Q_W and Q_{O1}.

to 2 mm over a length of 10 mm. Water droplets were generated at a $Q_W : Q_{O1}$ ratio of 1 : 5. The $Q_W : Q_{O1}$ ratio was kept constant to ensure that the droplets generated were of identical volumes. Four different hexadecane flow rates were studied, Q_{O1} = 10, 25, 50, 75 μL min^{-1}, where the respective water flow rates were Q_W = 2, 5, 10, 15 μL min^{-1}. Q_{O2} was systematically increased to decrease α_D, and the flow of droplets through the 3D microchannel was observed to see if the droplets self-assembled into ordered and closed packed structures. The results are shown in Fig. 2. The total flow rate is plotted against α_D, where an increase in Q_{O2} resulted in a decrease in α_D and an increase in the total flow rate. For each combination of Q_W and Q_{O1} studied, there existed a critical α_D below which self-assembly of droplets did not occur. For Q_{O1} = 10, 25, 50, 75 μL min^{-1}, self-assembly of droplets did not occur when α_D was less than 0.062, 0.047, 0.038, and 0.032 respectively. Our experiments suggested that the critical α_D required for self-assembly was lowered when water droplets were generated at higher Q_W and Q_{O1}. It is important to note that an increase in Q_{O1} results in an increased velocity of hexadecane within the microchannel for a given α_D. We tentatively hypothesize at higher Q_W and Q_{O1}, the droplets experience a higher drag which favors jamming and self-assembly. Therefore, at higher Q_W and Q_{O1}, a higher dilution flowrate Q_{O2} (equivalently a lower α_D) is required to prevent self-assembly.

Self-assembly of 3D ordered emulsions

In the previous sections, we demonstrated that the 3D microchannels allowed for self-assembly of 2D ordered emulsions over a wide range of volume fractions of droplets. This observation suggested that rationally designed, 3D microchannels might provide better control over self-assembly of emulsions than 2D microchannels. While ordered 3D self-assembly of droplets are desired in some applications, it is still difficult to achieve it inside planar devices, and there have been only a few demonstrations. Hatch and co-workers showed the predictive assembly of 2D and 3D lattices of droplets by controlling the ratio of microchannel height to droplet diameter.[17] Wang and co-workers varied ϕ_D along the length of the microchannel by incorporating capillary drainage channels for the continuous phase.[32] In their experiments droplets self-assembled into different structures along the length of the microchannel. At locations of high ϕ_D, the self-assembly of 2D and 3D lattices could be predicted by the theoretical framework developed by Hatch and co-workers. While there have been a couple of demonstrations of self-assembly of 3D lattices of droplets and bubbles in 3D microchannels, these experimental studies have shown that both disordered and ordered structures are favored in 3D microchannels.[6,9]

Our objective here was to demonstrate the self-assembly of droplets into ordered 3D lattices by the use of 3D microchannels. Fig. 3a shows the schematic illustration of the 3D microfluidic device used. Aqueous droplets were generated in hexadecane at Q_{O1} = 75 μL min^{-1} and Q_W = 15 μL min^{-1}. Hexadecane containing a dissolved surfactant was used as the continuous phase to prevent the coalescence of the water droplets. We gradually increased α_D by increasing the hexadecane withdrawal flow rate Q_{O2} from 0 to −70 μL min^{-1}. The minus sign here indicated the withdrawal of hexadecane from the microchannel. As the continuous phase was withdrawn, α_D was increased from 0.167 to 0.75. α_D, the fraction of the injected dispersed phase was calculated as $\alpha_D = Q_W/(Q_W + Q_{O1} + Q_{O2})$. Fig. 3b–h show microscopic images of self-assembled droplets at α_D = 0.167, 0.25, 0.375, 0.535, 0.6, 0.667, 0.75. The corresponding ϕ_D was approximately 0.26, 0.3, 0.39, 0.52, 0.6, 0.68, 0.75. ϕ_D, the volume fraction of the dispersed phase was calculated as $\phi_D = nV_D/Lwh$, where n is the number of droplets in length L of the microchannel, V_D is the volume of a single droplet, and w, h, are the widths and heights of the microchannel. V_D was calculated as the volume of a sphere of diameter d, where d was measured directly from the microscopic images of the droplets. Our measurements suggested that while at low α_D the continuous phase had a higher average velocity than the droplets, for $\alpha_D > 0.375$ the flow was homogeneous, and the droplets and the continuous phase had roughly the same velocity. The gradual increase in the ϕ_D resulted in self-assembly of droplets into ordered 3D arrays (Fig. 3b–h). At low ϕ_D, a single layer of ordered emulsions was observed (Fig. 3b). A transition from a single layer to multiple layers of ordered emulsions was observed as ϕ_D was gradually increased (Fig. 3c–h). At specific values of ϕ_D, defect-free, ordered emulsions were assembled in two and three layers (Fig. 3e and h). These experiments demonstrated that controlled self-assembly of multilayer emulsions could be achieved in 3D microchannels by gradually increasing α_D to increase ϕ_D.

Hatch and co-workers predicted and experimentally confirmed in 2D microchannels that the lattice patterns of the self-assembled

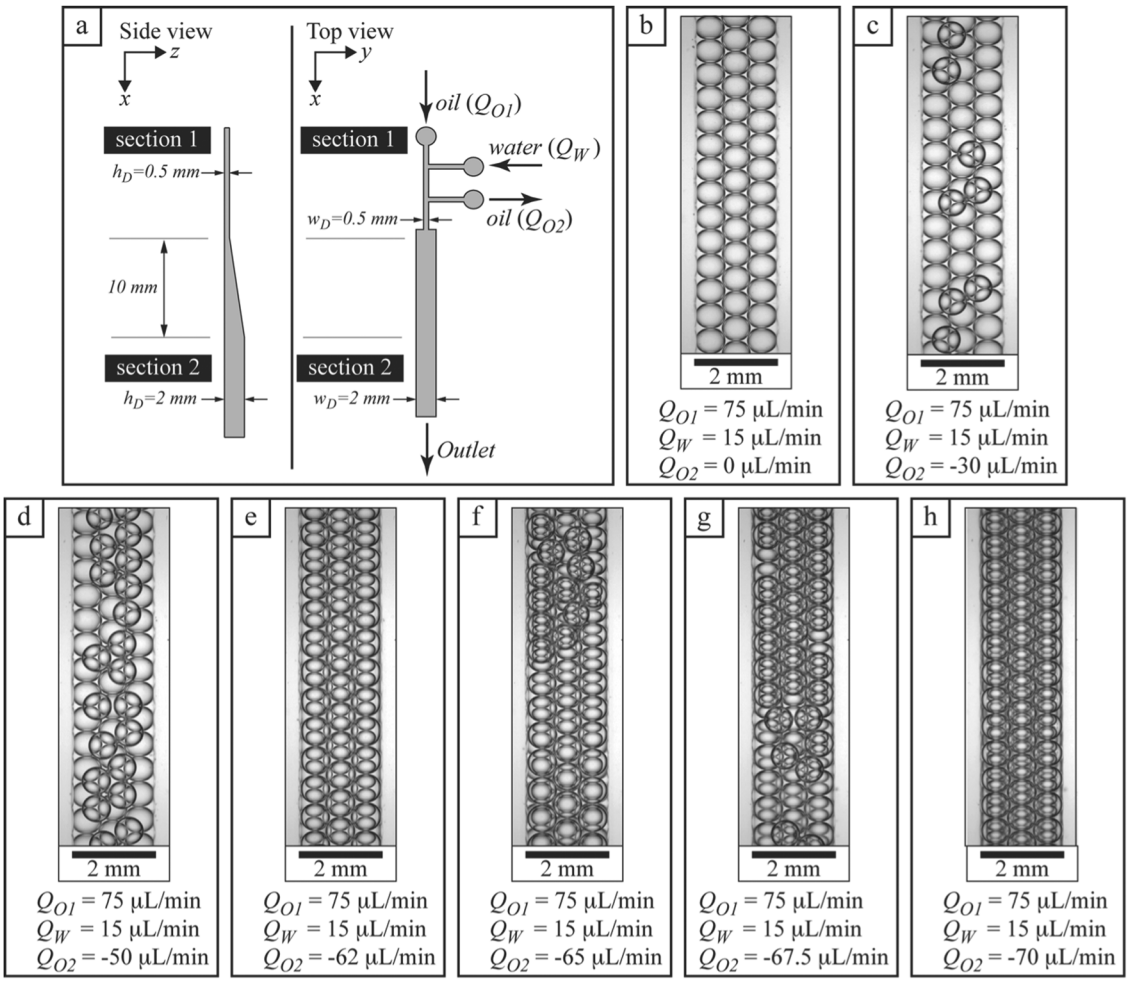

Fig. 3 (a) Schematic illustration of 3D microfluidic devices used for self-assembly of water droplets into 2D and 3D ordered arrays. (b–h) Microscopic images of self-assembled droplets in section 2 at α_D = 0.167, 0.25, 0.375, 0.535, 0.6, 0.667, 0.75. Droplets were generated at the same rates of flow at the T-junction (Q_{O1} = 75 μL min^{-1}, Q_W = 15 μL min^{-1}). Oil was withdrawn through the oil outlet to increase α_D. Increase in α_D resulted in the increase of ϕ_D. $\phi_D \sim$ 0.26, 0.3, 0.39, 0.52, 0.6, 0.68, 0.75. Increasing ϕ_D promoted the self-assembly of ordered, multilayer arrays of microfluidic droplets. Complete one (a), two (e), and three (h) layer ordered arrays of droplets were self-assembled by gradually increasing ϕ_D.

droplets depended exclusively on the ratio of the microchannel height to the droplet diameter (h/D). Their calculations were based on equilibrium states. Different h/D ratios led to different 2D and 3D lattices.[17] In our experiments with 3D microchannels, we found that the single, double and triple layers of droplets could be assembled at the same h/D ratio for different ϕ_D. This observation suggested the importance of hydrodynamics on the self-assembly of droplets in 3D microchannels. Furthermore, past studies on the self-assembly of 3D lattices in 3D microchannels showed highly disordered arrangements of droplets at certain ϕ_D.[6,9] Our experiments demonstrated that gradual increase in ϕ_D allowed achieving the self-assembly of highly ordered 2D and 3D lattices of droplets.

Path dependent self-assembly of ordered emulsions

In the previous sections, we demonstrated the use of 3D microchannels to control the self-assembly of droplets into ordered 2D and 3D arrays. Studies on self-assembly of droplets in microfluidic devices have demonstrated that for a microchannel of a given width and height, self-assembly is controlled by the size of droplets, the volume fraction of droplets, and the dimensions of the microchannels.[2–4,6–9,17,31] In this section, we exploited the ability to fabricate 3D microchannels to demonstrate that the assembly of droplets into ordered emulsions depended on how they were assembled. Specifically, we found that the self-assembly of emulsions was dictated not only by the geometry of microchannels but also by changes in the geometry of the microchannel. We describe this phenomenon as path dependent self-assembly.

Fig. 4a and b shows the schematic illustrations of the devices used. Water droplets in hexadecane were generated at a T-junction and flowed into a section where the microchannel width and height was increased to 2 mm. Hexadecane containing a dissolved surfactant was used as the continuous phase to prevent the coalescence of the water droplets. To highlight the difference in the self-assembly of the droplets in 3D channels, we fabricated two types of microfluidic devices. In Device 1, the width and height were increased in a single discontinuous step (Fig. 4a). In Device 2, the width was increased in a single step,

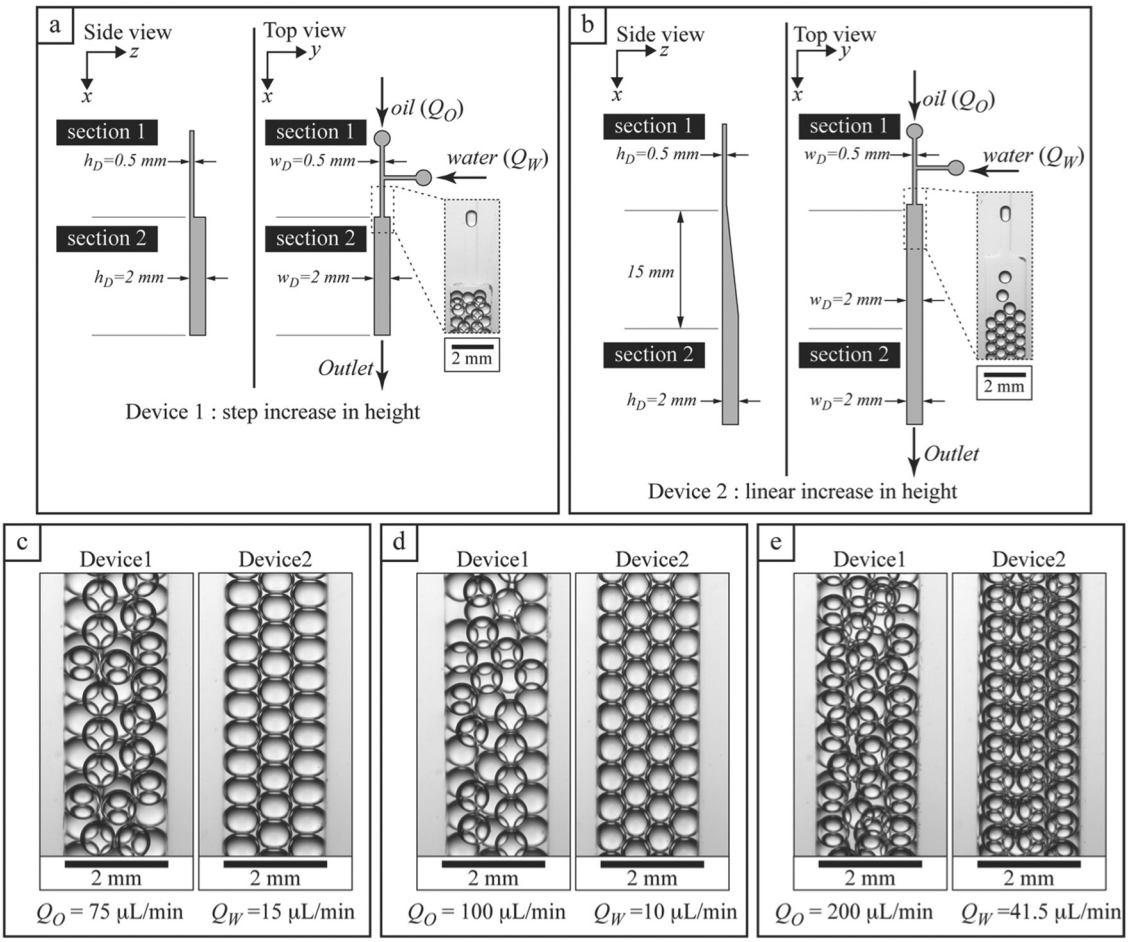

Fig. 4 (a and b) Schematic illustrations of devices used to study the dependence microfluidic emulsion assembly on microchannel geometry. (c–e) Stereomicroscopic images of assembled emulsions in section 2. In Device 1, defect-free ordered arrays of droplets did not form. In contrast, Device 2 allowed for the defect-free assembly of 2D (c and d) and 3D (e) ordered arrays of droplets.

and the height was linearly increased from 0.5 mm to 2 mm over a length of 15 mm (Fig. 4b).

While the dimensions of the expanded sections (*i.e.* chambers where the assembly of droplets occurred) were identical in both devices, the self-assembly of droplets in these devices were remarkably different. In Device 1, the droplets did not assemble into ordered structures. In Device 2, at similar flow conditions, the droplets assembled into ordered emulsions. In Device 2, the changes in the velocity of flow was gradual. We hypothesized that abrupt changes in velocity at the expansion led to disordered assembly in Device 1, while gradual changes in velocity of flow led to the formation of ordered emulsions in Device 2. To the best of our knowledge, this is the first demonstration that 3D assembly of emulsions can be ensured by the appropriate design of 3D microchannels.

Remarks on generality of method

In all experiments described thus far, we used water droplets in hexadecane to illustrate the ability of 3D microchannels to promote the self-assembly of droplets into ordered water-in-oil emulsions. In this section, we studied the ability of 3D microchannels to achieve self-assembly of ordered oil-in-water emulsions and ordered foams. Droplets and bubbles were generated at a T-junction and were directed into a microchannel where the width was increased to 2 mm in a single step and height was increased linearly to 2 mm over a length of 15 mm. Water containing a dissolved surfactant was used as the continuous phase to prevent the coalescence of the hexadecane droplets and air bubbles. The 3D microchannel promoted the self-assembly of both hexadecane droplets in water and air bubbles in water into ordered emulsions and foams respectively. The self-assembled oil-in-water emulsions and foams in the 3D microchannel are shown in Fig. 5.

Our experiments demonstrated that 3D microchannels can be used to promote self-assembly in systems where the density ratio $\rho_R > 1$ and in systems where $\rho_R < 1$ where ρ_R is the ratio of the density of the dispersed phase to that of the continuous phase. It is our hypothesis that, in systems with $\rho_R > 1$, the droplets sink to the bottom of the microchannel where they concentrate, jam and self-assemble into ordered structures. Conversely in systems with $\rho_R < 1$, we hypothesized that the bubbles or droplets would float to the top of the microchannel, where they again concentrate, jam and self-assemble into ordered structures. In the current experiments, the density of the dispersed phase was at least 20% greater or lesser than the

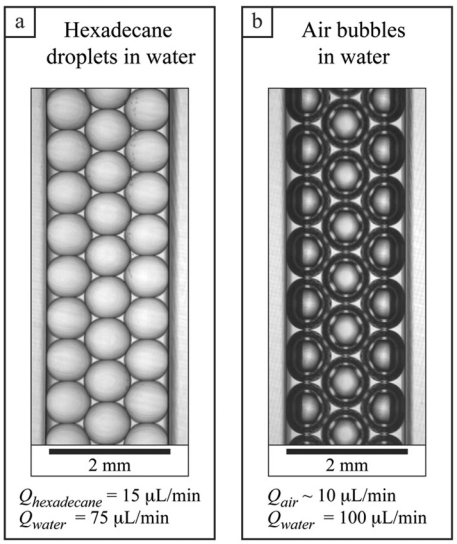

Fig. 5 (a) Photomicrograph of hexadecane droplets self-assembled into ordered oil-in-water emulsions using 3D microchannels. (b) Photomicrograph of air bubbles self-assembled into ordered foams using 3D microchannels. The flowrates used to generate the droplets and bubbles are given in the figure; no additional water was injected to the system.

continuous phase. While we have not explored systems where the difference in densities of the dispersed and continuous phase is smaller than 20%, self-assembly of droplets or bubbles into ordered structures is likely to be inhibited when ρ_R gets close to 1, where the critical values are to be investigated.

Our experiments also demonstrated that 3D microchannels can be used to self-assemble droplets and bubbles into ordered foams and emulsions in systems where the viscosity ratio (μ_R) ranges from ~0.005 to 3.45. μ_R is the ratio of the dynamic viscosity of the dispersed phase to that of the continuous phase. Currently in our experiments the dynamic viscosity of the continuous phase is on the order of 1 mPa s. In systems where the viscosity of the continuous phase is larger than 1 mPa s, we expect that the lateral rearrangement of bubbles and droplets would slow down by viscous drag force, and the self-assembly would be eventually prohibited.

In all our experiments we ensured that the continuous phase preferentially wetted the microchannel wall. In the previous sections, experiments with water droplets in hexadecane were carried out in hydrophobic microchannels. Experiments with hexadecane droplets in water and air bubbles in water were carried out in hydrophilic microchannels. In our experiments with 3D microchannels, droplets and bubbles were unconfined (*i.e.* maintaining spherical shapes), and they either sank down to the bottom of the channel or rose up to the top of the microchannel depending on the value of ρ_R. Herein, it is crucial to ensure that the continuous phase wets the microchannel walls preferentially over the dispersed phase. Otherwise, droplets or bubbles would be stuck to the microchannel walls and the steady flow would be disturbed.

Microfluidic extrusion of fibers with ordered macropores

With potential applications in tissue engineering and drug delivery, microfibers have received much attention recently.[33,34] Continuous fabrication of microfibers has been achieved in

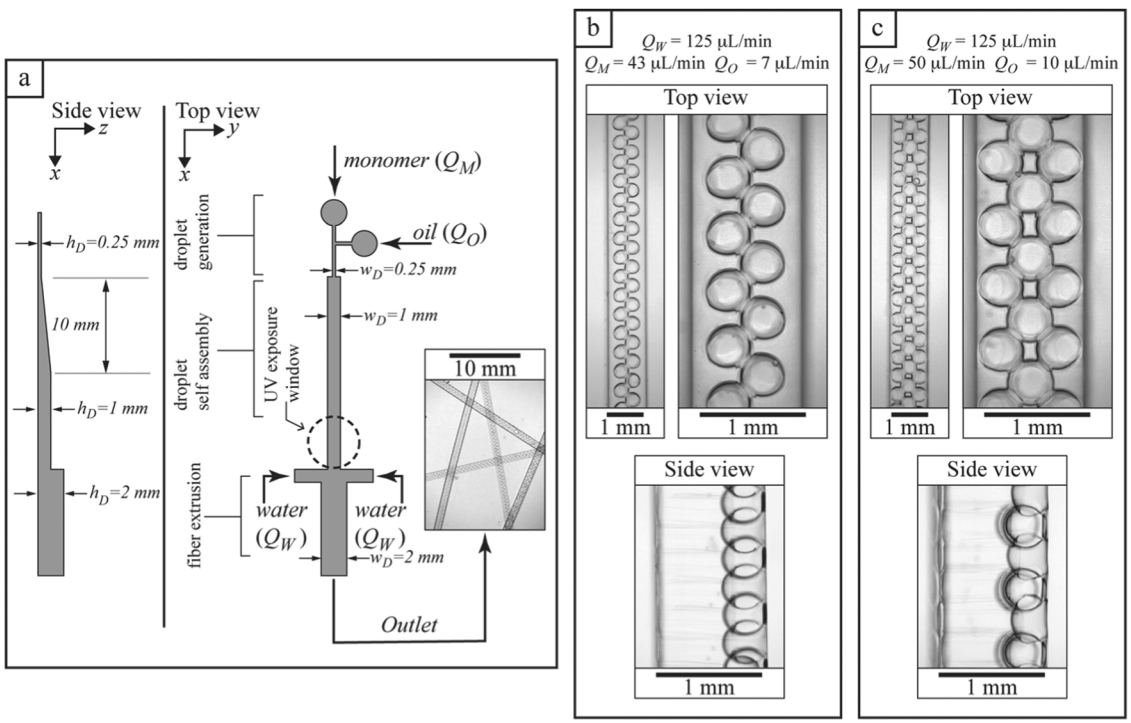

Fig. 6 (a) Schematic illustration of 3D microfluidic device used for the synthesis of macroporous hydrogel fibers. (a-inset) Wide field microscopic images of extruded fibers collected at the outlet. (b and c) Microscopic images of extruded fibers with different porous structures. For each fiber, two representative top-view photomicrographs at two different magnifications and a single side-view photomicrograph are shown. The side view photomicrographs show that the fibers have an anisotropic porous structure with the macropores confined to a single surface.

microfluidic devices in a facile manner.[33–42] Herein, the ability to fabricate fibers with tailored anisotropy in shape, structure and composition is highly sought after.[38–40,42] In this section, we demonstrated the use of self-assembled droplets as a template for the fabrication of hydrogel fibers with ordered macropores. 3D microchannels were used to ensure the formation of 2D lattices of droplets that were subsequently used as a template for the syntheses of porous hydrogel fibers. The use of 3D microchannels allowed for fabrication of microfibers with ordered macropores anisotropically located within the fiber. In our demonstration, the pores were confined to a single surface of the fiber.

Fig. 6a shows the schematic illustration of the microfluidic device used, and details of the experiment are given in the materials and methods section. In brief, droplets of hexadecane in the monomer solution were generated at a T-junction. These droplets were self-assembled into 2D arrays, and subsequently the monomer solution was polymerized. During the experiment, the microfluidic device was placed in a Petri dish filled with water and the extruded fibers were directly collected in water. The self-assembled 2D array of droplets served as a template for the macropores. In our experiments, after polymerization, holes were observed both in between the adjacent cells and at the surface of the fiber. As a consequence, after the polymerization, the hexadecane droplets were not completely encased by the hydrogel matrix and were readily removed when rinsed with water. We hypothesized that the film of monomer solution between adjacent droplets and between the droplets and the microchannel wall ruptured during the polymerization. Such open cellular structures have been reported in previous studies of polymerization of high internal phase emulsions; therein, formation of holes between cells has been attributed to the contraction of thin monomer films during polymerization.[43,44]

Fig. 6b and c show optical micrographs of the hydrogel fibers with ordered macropores stored in water after the polymerization. Arrangement of pores were controlled by changing rates of flow of the monomer solution (Q_M) and hexadecane (Q_O) to assemble droplets into 2D arrays with different configurations. These self-assembled 2D arrays of droplets subsequently acted as templates for the macropores. The use of 2D arrays of droplets (with the droplet diameter smaller than microchannel height) ensured that the synthesized hydrogels had an anisotropic structure. The self-assembled 2D array of droplets were confined to the top surface of the microchannel as the hexadecane droplets were lighter than aqueous monomer solution surrounding them. Consequently, after the removal of the droplets in the extruded fibers the macropores were localized to one side of the fiber.

Conclusions

In this paper, we discussed the utility of 3D microchannels in the self-assembly of droplets into ordered 2D and 3D lattices. 3D microchannels were fabricated by soft lithography with the use of 3D printed molds. 2D arrays of droplets were assembled at low volume fractions of the dispersed phase, and controllable assembly of 3D arrays of droplets was carried out by gradually increasing the volume fraction of the dispersed phase. Our study suggested that self-assembly of microfluidic droplets depended on the transitions in microchannel geometry, and not the geometry of the region of droplet assembly. Microchannels with a linear increase in height performed better in guiding droplets into ordered 2D and 3D arrays than microchannels with a step change in height. Lastly, we have used self-assembled droplets in 3D microchannels as a template to extrude hydrogel microporous fibers with tailored anisotropy in the structure.

Our studies demonstrated that 3D microchannels were an excellent platform to engineer ordered foams, emulsions, and complex multiphase materials with unprecedented control over internal morphologies. In our current experiments, we generated droplets with diameters on the order of 100 μm and assembled them into ordered emulsions with lateral dimensions on the order of 1 mm. As such, our experiments are relevant to the continuous fabrication of mechanical metamaterials and solid foams for thermal and acoustic applications. The size of the droplets that we generated was governed by the size of microchannels we were able to fabricate using 3D printing. Currently available commercial stereolithography and polymer jetting printers have a typical lateral resolution on the order of 100 μm. While photolithography offers much higher resolutions, they are not a convenient solution to fabricate microchannels with 3D features. Recent advents in additive manufacturing have opened up an avenue to fabricate feature sizes on the order of 10 μm,[45] and methods such as two-photon polymerization allows to fabricate features with resolutions of 1 μm.[46] While our demonstrations are based on the devices that are readily fabricated using consumer-grade desktop 3D printers, it is our belief that 3D microchannels enabled by advanced additive manufacturing should offer 3D assembly of droplets in the order of 1 μm to 10 μm. Such size scale would facilitate the fabrication of complex biomimetic hierarchical materials and tissue engineering scaffolds.

Materials and methods

3D printing of soft lithography molds

AutoCAD was used to design the molds and the designs were exported as STL files. Molds for the microfluidic devices were fabricated using either Objet30 Prime or Objet24 3D printer (Stratasys Ltd, USA). Proprietary resins (Veroclear or Verowhite) were used and the molds were printed in 28 μm layers using the glossy mode. In the glossy mode, a layer of support material is first printed, and subsequently the entire part is printed on top without any further use of support material. After printing, the layer of support material at the bottom of the printed part was removed by rinsing thoroughly with water. The cleaned molds were then soaked in DI water for 2 hours. The mold was subsequently dried with compressed air and placed in an oven at 60 °C for 48 hours. This post-processing was carried out to ensure that PDMS does not stick to the molds during the replication.

Replication of microchannels in PDMS

A 10 to 1 weight ratio of PDMS base and curing agent (Sylgard 184, silicone elastomer kit, Dow Corning, USA) was thoroughly

mixed and degassed under vacuum to remove bubbles. The mixture was then poured into 3D printed molds and placed in an oven or hotplate set at 60 °C for at least 3 hours. The PDMS replicas were then carefully peeled off from the masters. For experiments in droplet formation and self-assembly, two different microfluidic devices were fabricated. For experiments involving the generation of water droplets a hydrophobic PDMS on glass microfluidic devices were fabricated. For experiments involving the generation of hexadecane droplets in water, and air bubbles in water, hydrophilic PDMS on glass microfluidic devices were used. In experiments involving the generation of monomer droplets in water (used in the extrusion of fibers), hydrophilic PDMS on PDMS microfluidic devices were used. Hydrophobic devices were fabricated *via* air plasma treatment (Harrick Plasma PDC 32G, USA) to seal the replicated PDMS microchannels to a glass slide. Alternatively, a corona discharge (model BD-20, Electro Technic Products Inc., USA) was used to treat the surfaces to enable bonding. The sealed device was placed in an oven or hotplate set at 60 °C for at least 6 hours to ensure that the device is hydrophobic. Hydrophilic devices were fabricated *via* air plasma treatment or corona discharge treatment to enable bonding of the surfaces. For experiments with hexadecane droplets in water or air bubbles in water, the replicated microchannels were sealed to glass slides. For microfluidic fiber extrusion experiments the replicated PDMS microchannels were sealed to a flat slab of PDMS. The sealed device was immediately filled with water and used within 15 minutes. PDMS microchannels were fabricated with at least a 3 mm thick roof (the thickness of the PDMS layer above the microchannel) to avoid any deformation of the cross section of the channel due to sagging or internal pressure.

Droplet self-assembly

Hydrophobic microfluidic devices were used for experiments with water droplets in hexadecane, while hydrophilic microfluidic devices were used for experiments with hexadecane droplets in water and air bubbles in water. Molds for the microfluidic devices were fabricated using either Objet30 Prime or Objet24 3D printer (Stratasys Ltd, USA). For water-in-oil experiments, water was used as the dispersed phase, while a 2.5% (v/v) solution of Span 80 (Sigma Aldrich, Singapore) in hexadecane (Sigma Aldrich, Singapore) or 2.5% (v/v) solution of sorbitan oleate (MakingCosmetics, USA) in hexadecane (Acros Organics, USA) was used as the continuous phase. For oil-in-water experiments hexadecane (Acros Organics, USA) was used as the dispersed phase, and a 2.5% solution of polysorbate 20 (MakingCosmetics, USA) in water was used as the continuous phase. Water containing 2.5% (v/v) of polysorbate 20 was also used as the continuous phase in experiments with air bubbles. PTFE tubes with 0.032 inch diameter and 0.056 inch outer diameter was used to connect the liquid filled syringes to the microfluidic devices. Syringe pumps were used to pump the dispersed and continuous phases at the required flow rates. In experiments with air bubbles, in order to pump air, the syringe was filled with glycerol and the PTFE tube connecting the syringe and the microfluidic device was left air filled. Pumping glycerol from the syringe using syringe pumps displaced air from the tube into the microfluidic device. For experiments involving droplets, PTFE tubes were used as outlets. For experiments involving air bubbles, the outlet consisted of a rectangular hole of 3 mm × 5 mm. A stereo microscope (Leica MZ125, Leica Microsystems, Germany) with a CCD camera (Basler ac2040-90uc, Basler AG, Germany), Optem Fusion 7:1 zoom system (QiOptic, UK), with a CMOS camera (xiQ – MQ013CG, Ximea, Germany), or Computar MLM3X-MP video lens with a CMOS camera (xiQ – MQ013CG, Ximea, Germany) were used to visualize the flows and capture videos and photomicrographs. The details of the individual experiments are given below.

Self-assembly of 2D lattices of droplets – 2D *vs.* 3D microchannels. Hydrophobic microfluidic devices were used in these experiments. The microfluidic devices comprised of a section to assemble ordered emulsions located downstream of a T-junction droplet generator (Fig. 1a and b). The T-junction droplet generator was designed to have channels of square cross-section with width (w_D) = height (h_D) = 0.5 mm. Water droplets were generated in hexadecane (with 2.5% v/v Span 80). The rates of flows of water and hexadecane was Q_W and Q_{O1}, respectively. A second inlet located downstream of the T-junction was used to inject additional hexadecane at a flow rate of Q_{O2}. We controlled α_D by changing Q_{O2}; an increase in Q_{O2} resulted in the decrease α_D.

Critical α_D required for self-assembly. The microfluidic device used is identical to the 3D microfluidic used in the section ''Self-assembly of 2D lattices of droplets – 2D *vs.* 3D microchannels'' (Fig. 1b). Water droplets were generated in hexadecane (with 2.5% v/v sorbitan oleate). The rates of flows of water and hexadecane was Q_W and Q_{O1}, respectively. A second inlet located downstream of the T-junction was used to inject additional hexadecane at a flow rate of Q_{O2}. We controlled α_D by changing Q_{O2}; an increase in Q_{O2} resulted in the decrease α_D.

Self-assembly of 3D ordered emulsions. Hydrophobic microfluidic devices were used in these experiments. The microfluidic device consisted of a T-junction droplet generator consisting of channels with square cross-section with width (w_D) = height (h_D) = 0.5 mm (Fig. 3a). Water droplets were generated in hexadecane (with 2.5% v/v Span 80) at the T-junction. Water and hexadecane were infused at the flow rates Q_W and Q_{O1}, respectively. An outlet for hexadecane was located downstream of the T-junction; this additional outlet was used to selectively withdraw hexadecane at a flow rate of Q_{O2}. The removal of hexadecane enabled the increase of α_D. The generated droplets were directed to a section to perform self-assembly; the width of the channel was increased to 2 mm in a single step and the height was linearly increased from 0.5 mm to 2 mm over a length of 10 mm.

Path dependent self-assembly of ordered emulsions. Hydrophobic microfluidic devices were used in these experiments. The microfluidic devices used comprised of a section to assemble ordered emulsions located downstream of a T-junction droplet generator (Fig. 4a and b). The T-junction droplet generator was designed to have channels of square cross-section with width (w_D) = height (h_D) = 0.5 mm. Water droplets dispersed in hexadecane (with 2.5% v/v span 80) were generated at the T-junction, and the generated droplets subsequently flowed into the section where the width and height of the microchannel was increased to 2 mm.

Two different device designs were studied – in Device 1 the height was increased in a single step while in Device 2 the height was linearly increased.

Remarks on generality of method. Hydrophilic microfluidic devices were used in these experiments. The design of the microfluidic device used is identical to the Device 2 used in the section ''Path dependent self-assembly of ordered emulsions'' (Fig. 4b). In experiments involving oil-in-water emulsions, hexadecane droplets dispersed in water (with 2.5% v/v polysorbate 20) were generated at the T-junction, and the generated droplets were self-assembled into ordered structures in the microchannel section where the height was linearly increased to 2 mm. In experiments involving foams, air bubbles dispersed in water (with 2.5% v/v polysorbate 20) were generated at the T-junction, and the generated bubbles were self-assembled into ordered structures in the microchannel section where the height was linearly increased to 2 mm.

Microfluidic fiber extrusion

Hydrophilic microfluidic devices were used for these experiments. Molds for the microfluidic devices were fabricated using an Objet24 3D printer (Stratasys Ltd, USA). Hexadecane was used as the dispersed phase. A monomer solution was used as the continuous phase. The monomer solution was formulated by first dissolving 50% (v/v) of poly(ethylene glycol) diacrylate (M_n = 700 g mol^{-1}) in water and subsequently dissolving 5% (w/v) of sodium dodecylsulphate in the resultant solution. Immediately prior to carrying out experiments 1% (v/v) photoinitiator 2-hydroxy-2-methylpropiophenone (Darocur 1173) was added to the above solution. All chemicals were purchased from Sigma Aldrich and used as purchased. Syringe pumps were used to deliver the dispersed phase and continuous phase at the required flow rates to generate droplets of hexadecane dispersed in the monomer solution.

The microfluidic device used consisted of a T-junction droplet generator and sections for self-assembly of droplets and extrusion of fibers. The schematic illustration of the device is given (Fig. 6a). The T-junction droplet generator was designed to have channels of square cross-section with width (w_D) and height (h_D) of 0.25 mm. Hexadecane droplets dispersed in monomer solution were generated at the T-junction by pumping in monomer solution a flow rate of Q_M and the hexadecane at a flow rate of Q_O. The generated droplets subsequently flowed into the droplet self-assembly section. The width of the microchannel was increased to 1 mm in a single step, and height of the microchannel was linearly increased to 1 mm over the length of 10 mm, followed by a straight microchannel of length of 10 mm. The straight channel was designed to have a constant width and height (w_D = h_D = 1 mm). At the end of this section, the assembled droplets in the monomer solution were exposed to a collimated UV source through a 4 mm diameter window. The UV exposure window was fabricated by punching a 4 mm hole through a UV opaque film. A collimated 365 nm wavelength LED (M365L2, Thor Labs, USA) was used as the UV source. The UV exposure window was aligned properly and placed directly on the microfluidic device, and the UV source was placed on top of the window to carry out polymerization. The monomer solution was polymerized, and the hydrogel fiber containing encased hexadecane droplets were extruded into a microchannel where the width and height was increased to 2 mm in a single step. Two additional inlets were used to pump in water at a flow rate of Q_W to continuously wash the extruded fibers. The extruded fibers were rinsed thoroughly with water to remove the encased hexadecane droplets, and subsequently were stored in water. Photomicrographs of the extruded fibers were captured by Optem Fusion 7:1 zoom system (QiOptic, UK) fitted with a CMOS camera (xiQ – MQ013CG, Ximea, Germany).

Image enhancement

Adobe Photoshop was used to enhance all photomicrographs. The photomicrographs were first converted to grayscale and the brightness and contrast was adjusted. An ''Auto Level'' function was then employed to further enhance the photomicrographs.

Conflicts of interest

There are no conflicts to declare.

Acknowledgements

P. P. thanks the SUTD-MIT postdoctoral fellowship program. M. H. thanks financial support from Start-up Research Grant (SREP14088), and Digital Manufacturing and Design (DManD) Center (RGDM1620403) at Singapore University of Technology and Design. The authors thanks the International Design Center at Massachusetts Institute of Technology for the shared equipment.

References

1 T. Thorsen, R. W. Roberts, F. H. Arnold and S. R. Quake, *Phys. Rev. Lett.*, 2001, **86**, 4163–4166.
2 P. Garstecki, I. Gitlin, W. DiLuzio, G. M. Whitesides, E. Kumacheva and H. A. Stone, *Appl. Phys. Lett.*, 2004, **85**, 2649–2651.
3 J. H. Xu, S. W. Li, Y. J. Wang and G. S. Luo, *Appl. Phys. Lett.*, 2006, **88**, 133506.
4 S. M. Vuong and S. L. Anna, *Biomicrofluidics*, 2012, **6**, 022004.
5 D. R. Link, S. L. Anna, D. A. Weitz and H. A. Stone, *Phys. Rev. Lett.*, 2004, **92**, 054503.
6 T. Cubaud, M. Tatineni, X. Zhong and C.-M. Ho, *Phys. Rev. E: Stat., Nonlinear, Soft Matter Phys.*, 2005, **72**, 037302.
7 M. Seo, Z. Nie, S. Xu, P. C. Lewis and E. Kumacheva, *Langmuir*, 2005, **21**, 4773–4775.
8 M. Hashimoto, B. Mayers, P. Garstecki and G. M. Whitesides, *Small*, 2006, **2**, 1292–1298.
9 C. Priest, S. Herminghaus and R. Seemann, *Appl. Phys. Lett.*, 2006, **88**, 024106.
10 J. P. Raven and P. Marmottant, *Phys. Rev. Lett.*, 2006, **97**, 154501.
11 M. Hashimoto, P. Garstecki and G. M. Whitesides, *Small*, 2007, **3**, 1792–1802.
12 J. P. Raven and P. Marmottant, *Phys. Rev. Lett.*, 2009, **102**, 084501.
13 E. Surenjav, C. Priest, S. Herminghaus and R. Seemann, *Lab Chip*, 2009, **9**, 325–330.

14 E. Surenjav, S. Herminghaus, C. Priest and R. Seemann, *Appl. Phys. Lett.*, 2009, **95**, 154104.
15 P. Garstecki and G. M. Whitesides, *Phys. Rev. Lett.*, 2006, **97**, 024503.
16 Y. Gai, C. M. Leong, W. Cai and S. K. Y. Tang, *Proc. Natl. Acad. Sci. U. S. A.*, 2016, **113**, 12082–12087.
17 A. C. Hatch, J. S. Fisher, S. L. Pentoney, D. L. Yang and A. P. Lee, *Lab Chip*, 2011, **11**, 2509–2517.
18 P. Mary, A. R. Abate, J. J. Agresti and D. A. Weitz, *Biomicrofluidics*, 2011, **5**, 024101.
19 M. Kim, M. Pan, Y. Gai, S. Pang, C. Han, C. Yang and S. K. Y. Tang, *Lab Chip*, 2015, **15**, 1417–1423.
20 S. Duraiswamy and S. A. Khan, *Nano Lett.*, 2010, **10**, 3757–3763.
21 J. H. Kim, J.-H. Choi, J. Y. Sim, W. C. Jeong, S.-M. Yang and S.-H. Kim, *Langmuir*, 2014, **30**, 5404–5411.
22 S. Thutupalli, S. Herminghaus and R. Seemann, *Soft Matter*, 2011, **7**, 1312–1320.
23 Y. Elani, A. J. Demello, X. Niu and O. Ces, *Lab Chip*, 2012, **12**, 3514–3520.
24 K. Ma, R. Liontas, C. A. Conn, G. J. Hirasaki and S. L. Biswal, *Soft Matter*, 2012, **8**, 10669–10675.
25 R. Liontas, K. Ma, G. J. Hirasaki and S. L. Biswal, *Soft Matter*, 2013, **9**, 10971–10984.
26 N. Quennouz, M. Ryba, J.-F. Argillier, B. Herzhaft, Y. Peysson and N. Pannacci, *Oil Gas Sci. Technol.*, 2014, **69**, 457–466.
27 C. Micheau, E. Rosenberg, L. Barré and N. Pannacci, *Colloids Surf., A*, 2016, **501**, 122–131.
28 P. Marmottant and J.-P. Raven, *Soft Matter*, 2009, **5**, 3385–3388.
29 A. Huerre, V. Miralles and M.-C. Jullien, *Soft Matter*, 2014, **10**, 6888–6902.
30 L. Shui, E. Stefan Kooij, D. Wijnperle, A. van den Berg and J. C. T. Eijkel, *Soft Matter*, 2009, **5**, 2708–2712.
31 O. Claussen, S. Herminghaus and M. Brinkmann, *Phys. Rev. E: Stat., Nonlinear, Soft Matter Phys.*, 2012, **85**, 061403.
32 J. Wang, M. Jin, T. He, G. Zhou and L. Shui, *Micromachines*, 2015, **6**, 1331–1345.
33 H. Onoe and S. Takeuchi, *Drug Discovery Today*, 2015, **20**, 236–246.
34 J. Xue, Y. Niu, M. Gong, R. Shi, D. Chen, L. Zhang and Y. Lvov, *ACS Nano*, 2015, **9**, 1600–1612.
35 S.-J. Shin, J.-Y. Park, J.-Y. Lee, H. Park, Y.-D. Park, K.-B. Lee, C.-M. Whang and S.-H. Lee, *Langmuir*, 2007, **23**, 9104–9108.
36 C. M. Hwang, A. Khademhosseini, Y. Park, K. Sun and S. H. Lee, *Langmuir*, 2008, **24**, 6845–6851.
37 K. H. Lee, S. J. Shin, Y. Park and S.-H. Lee, *Small*, 2009, **5**, 1264–1268.
38 J.-H. Jung, C.-H. Choi, S. Chung, Y.-M. Chung and C.-S. Lee, *Lab Chip*, 2009, **9**, 2596–2602.
39 C.-H. Choi, H. Yi, S. Hwang, D. A. Weitz and C.-S. Lee, *Lab Chip*, 2011, **11**, 1477–1483.
40 M. Yamada, S. Sugaya, Y. Naganuma and M. Seki, *Soft Matter*, 2012, **8**, 3122–3130.
41 Y. Jun, E. Kang, S. Chae and S.-H. Lee, *Lab Chip*, 2014, **14**, 2145–2160.
42 W. Lan, Y. Du, X. Guo, A. Liu, S. Jing and S. Li, *Ind. Eng. Chem. Res.*, 2018, **57**, 212–219.
43 N. R. Cameron, D. C. Sherrington, L. Albiston and D. P. Gregory, *Colloid Polym. Sci.*, 1996, **274**, 592–595.
44 A. Testouri, M. Ranft, C. Honorez, N. Kaabeche, J. Ferbitz, D. Freidank and W. Drenckhan, *Adv. Eng. Mater.*, 2013, **15**, 1086–1098.
45 H. Gong, B. P. Bickham, A. T. Woolley and G. P. Nordin, *Lab Chip*, 2017, **17**, 2899–2909.
46 K.-S. Lee, R. H. Kim, D.-Y. Yang and S. H. Park, *Prog. Polym. Sci.*, 2008, **33**, 631–681.

